Decoupled aqueous batteries using pH-decoupling electrolytes

Yun-hai Zhu[1,2], *Yang-feng Cui*[1,3], *Zi-long Xie*[1,4], *Zhen-bang Zhuang*[1,2], *Gang Huang*[1] *and Xin-bo Zhang*[1,4] ✉

Abstract | Aqueous batteries have been considered as the most promising alternatives to the dominant lithium-based battery technologies because of their low cost, abundant resources and high safety. The output voltage of aqueous batteries is limited by the narrow stable voltage window of 1.23 V for water, which theoretically impedes further improvement of their energy density. However, the pH-decoupling electrolyte with an acidic catholyte and an alkaline anolyte has been verified to broaden the operating voltage window of the aqueous electrolyte to over 3 V, which goes beyond the voltage limitations of the aqueous batteries, making high-energy aqueous batteries possible. In this Review, we summarize the latest decoupled aqueous batteries based on pH-decoupling electrolytes from the perspective of ion-selective membranes, competitive redox couples and potential battery prototypes. The inherent defects and problems of these decoupled aqueous batteries are systematically analysed, and the critical scientific issues of this battery technology for future applications are discussed.

Non-aqueous Li-ion batteries (LIBs), characterized by high energy density (250–400 Wh kg^{-1}) and long cycle life (2,000–3,000 cycles), have been widely promoted to meet the global demand of portable electronic devices and electric vehicles[1,2]. However, the highly toxic and flammable organic electrolytes in LIBs raises potential safety and environmental concerns[2]. Aqueous batteries, in which non-flammable aqueous electrolytes replace organic electrolytes, have been considered as the ideal alternative to LIBs in the areas of electric vehicles and electrical energy-storage systems[3]. Nevertheless, the stable electrochemical stability window of water in aqueous electrolytes is only 1.23 V, beyond which undesired water splitting persists[4] (FIG. 1a). By contrast, continuous electrolyte decomposition does not occur in organic electrolytes, even when operating at a voltage beyond the operating voltage window of organic solvent. Generally, the degradation reactions of organic electrolytes are inhibited by the passivation films on the cathode and anode surface formed upon first charging by the decomposition of the electrolyte, which are known as the cathode–electrolyte interface and the solid–electrolyte interphase (SEI), respectively[5] (FIG. 1a). This SEI is practically unavailable in aqueous media because water hydrolysis only produces volatile gases, including oxygen (O_2) and hydrogen (H_2). Although the useful voltage range of aqueous electrolytes has been substantially expanded by the limited reaction kinetics of degradation reactions, it is still less than 2.0 V in most cases[6], thus making aqueous batteries insignificant and irrelevant.

In typical aqueous electrolytes, numerous water molecules — apart from those in a hydration shell — are non-coordinated and freely form hydrogen-bond networks with each other. In this case, water is highly active because the strength of the O–H covalent bond is weakened either by the hydrogen-bond interaction among water molecules or by the solvation between ions and water molecules[7]. Once the charge voltage is beyond the operating voltage window of the aqueous electrolytes, the water will split into H_2 and O_2 gas at the anode and cathode sides, respectively (FIG. 1b). To expand the electrochemically stable window of the aqueous electrolytes, it is critical to change the coordination environments of the water molecules, which can theoretically be achieved through electrolyte engineering[8–12]. Currently, a highly concentrated aqueous electrolyte (21 mol kg^{-1} lithium bis(trifluoromethane)sulfonimide (LiTFSI) aqueous electrolyte), dubbed water-in-salt electrolyte, was used as a new means to break through the voltage limitation of aqueous batteries[8]. In such super-concentrated aqueous electrolytes, the high population of anions forces them into the vicinity of the cation to form a novel anion-containing solvation sheath for Li^+ ion, which subsequently leads to a F-based SEI forming on the anode surface via anion reduction[13] (FIG. 1b). Furthermore, the electronegative anion species ($TFSI^-$) will absorb on the cathode surface during the charging process because of the effects of the electric field and the electrostatic force, thus forming a hydrophobic organic anion-rich double layer[14]. Such a hydrophobic layer repeals the

[1] State Key Laboratory of Rare Earth Resource Utilization, Changchun Institute of Applied Chemistry, Chinese Academy of Sciences, Changchun, China.

[2] Key Laboratory of Automobile Materials (Jilin University), Ministry of Education, Department of Materials Science and Engineering, Jilin University, Changchun, China.

[3] School of Materials Science and Engineering, Changchun University of Science and Technology, Changchun, China.

[4] University of Science and Technology of China, Hefei, China.

✉e-mail: xbzhang@ciac.ac.cn

https://doi.org/10.1038/s41570-022-00397-3

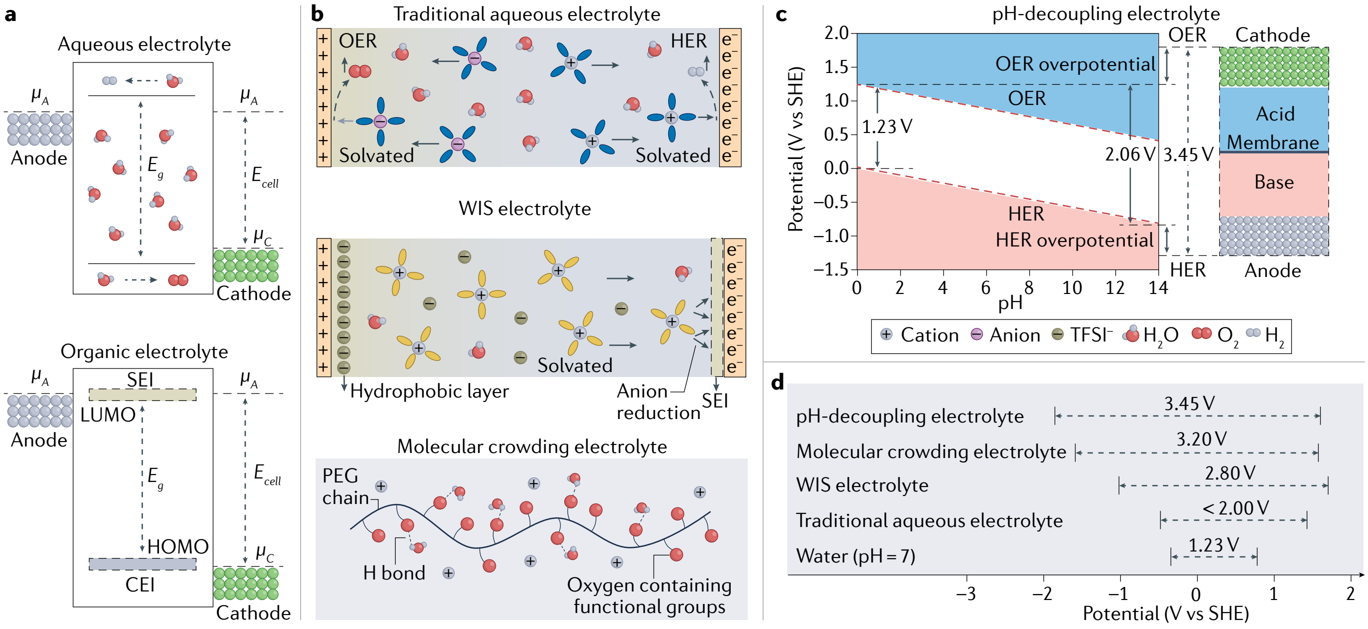

Fig. 1 | **Typical strategies for widening the operating voltage window of aqueous electrolytes. a** | Open-circuit energy diagram of an aqueous electrolyte and organic electrolyte. **b** | Water hydrolysis in traditional aqueous electrolyte (top) and suppressing water hydrolysis by water-in-salt (WIS) electrolytes (middle) and molecular crowding electrolytes (bottom). WIS electrolyte changes the solvation sheath structure of cation and molecular crowding electrolyte breaks the hydrogen-bonding network of water molecules. **c** | Pourbaix diagram of water and electrochemical principles for pH-decoupling electrolyte to widen the operating voltage window of aqueous electrolytes. **d** | Comparison of the operating voltage windows for various aqueous electrolytes. The pH-decoupling electrolyte is tested in a dual-electrolyte system with an alkaline $Zn/Zn(OH)_4^{2-}$ anode and an acidic MnO_2/Mn^{2+} cathode[17]. The molecular crowding electrolyte corresponds to 2 mol kg^{-1} LiTFSI-PEG (94 wt%)-water (6 wt%) electrolyte in a $Li_4Ti_5O_{12}//LiMn_2O_4$ cell[10]. The WIS electrolyte corresponds to a super-concentrated solute of 21 mol kg^{-1} LiTFSI electrolyte in a $Mo_6S_8//LiMn_2O_4$ cell[8]. μ_A, anode electrochemical potential; μ_C, cathode electrochemical potential; CEI, cathode–electrolyte interface; E_{cell}, battery voltage; E_g, electrolyte's electrochemical stability window; HER, hydrogen evolution reaction; HOMO, highest occupied molecular orbital; LUMO, lowest unoccupied molecular orbital, OER, oxygen evolution reaction; PEG, poly(ethylene glycol); SEI, solid–electrolyte interphase; SHE, standard hydrogen electrode; TFSI⁻, bis(trifluoromethane) sulfonimide anion.

adsorption of water molecules, consequently eliminating the oxygen evolution reaction (OER) (FIG. 1b). Notably, both the SEI and the hydrophobic double layer significantly widen the operating voltage window of the aqueous electrolyte.

Recently, another stability-enhancement effect for aqueous electrolytes was verified in the so-called molecular crowding electrolytes[10]. These molecular crowding electrolytes contain a mixed solvent, which includes low levels of water and high levels of crowding agents such as poly(ethylene glycol). The molecular crowding electrolytes trap and confine the water molecules within the crowding agent network and reconstruct hydrogen bonds between water molecules and the crowding agent as well (FIG. 1b). The newborn hydrogen-bond structure substantially suppresses the activity of water, such that water hydrolysis requires a much higher overpotential, namely, the electrochemical stability window of water widens. Both the water-in-salt electrolytes and the molecular crowding electrolytes could effectively extend the electrochemically stable window of aqueous electrolytes, but they come at a high cost and sluggish reaction kinetics. Theoretically, the potentials of the OER and the hydrogen evolution reaction (HER) could be easily adjusted by regulating pH, as they are heavily dependent on it[15], so the pH regulations of electrolytes are expected to stabilize aqueous electrolytes in a more facile way.

Recently, pH-decoupling electrolytes that simply couple a separated anolyte and catholyte with different pHs were proposed and studied, which were able to widen the operating voltage window of aqueous electrolyte more efficiently[12,16,17]. Theoretically, a pH-decoupling electrolyte with an acidic catholyte (pH = 0) and an alkaline anolyte (pH = 14) could enable an operating voltage window of up to 2.06 V, as illustrated in the Pourbaix diagram of water (FIG. 1c). Additionally, owing to the sluggish reaction kinetics for both acidic OER and alkaline HER, the electrochemical stability window of the pH-decoupling electrolyte could be further expanded to 3.45 V (REF.[17]) (FIG. 1d), making it possible for aqueous batteries to break through their voltage and energy density limitations.

To this end, a decoupled battery based on the pH-decoupling electrolyte has been used in the recent development of high-voltage aqueous batteries. In contrast to the common battery structure in which the cathode and anode are in one electrolyte, the decoupled battery has its cathode in an acidic catholyte and its anode in an alkaline anolyte, with an ion-selective membrane (ISM) to prevent chemical crossover between the acidic catholyte and the alkaline anolyte. The redox reactions on both the cathode and the anode sides are guaranteed by the mediator ions shuttling through the ISM. Notably, unlike the charge carriers

Ion-selective membrane

(ISM). A semipermeable membrane that has selective transmissibility to specific ions in solution.

Permselectivity
A term to define the preferential permeation of certain ionic species through ion-exchange membranes.

Donnan equilibrium
Also known as the Gibbs–Donnan effect, the behaviour of charged particles near a semipermeable membrane, which sometimes fail to distribute evenly across the two sides of the membrane.

in common batteries, the mediator ions in a decoupled battery generally do not participate in reactions involving the cathode and the anode. In this Review, we explore the state-of-the-art developments in the key components of the decoupled battery, focusing mainly on ISMs and competitive redox couples. We also present an overview of potential high-voltage decoupled battery prototypes and point out the remaining roadblocks, with a prospective discussion on the fundamental research and industrial implementation.

Ion-selective membranes

The essential prerequisite for the long-time operation of the decoupled battery is that the two electrodes work independently in their respective environments, which requires suppressing the crossover of hydrogen (H^+) and hydroxyl (OH^-) ions. Ion-exchange membranes (IEMs) are commonly applied in electrodialysis or diffusion dialysis to selectively transport specific cations or anions by means of an electrical potential or concentration gradient[18–20]. This selective transport is meant to prevent acid–base neutralization and keep ion conduction inside the decoupled battery[21,22]. IEMs mainly consist of hydrophobic polymer substrates, fixed ion-functionalized groups and mobile counterions, which are broadly segmented into cation-exchange membranes (CEMs) and anion-exchange membranes (AEMs), according to the type of ionic groups[23]. Generally, after sufficient water penetrates into the membranes, the ionic groups fixed on the hydrophobic polymer chains will ionize and release cations or anions, thereby conducting corresponding ions through the ionized groups with an opposite charge[23] (FIG. 2A,B). The ionic permselectivity of the IEM is rooted in Donnan equilibrium rather than the electrostatically repulsing or physically clogging of specific ions[24]. Under such a conduction mechanism, the IEMs are insufficient to shield the crossover of H^+ and OH^-, especially for a long time over several months or even several years. The solid inorganic electrolyte (SIE) membrane is another type of ISM used in the decoupled battery[25,26]. Generally, ionic transport in SIEs depends on the concentration and distribution of defects[27,28] (FIG. 2C). According to the Schottky and Frenkel point defects, the ion diffusion mechanisms

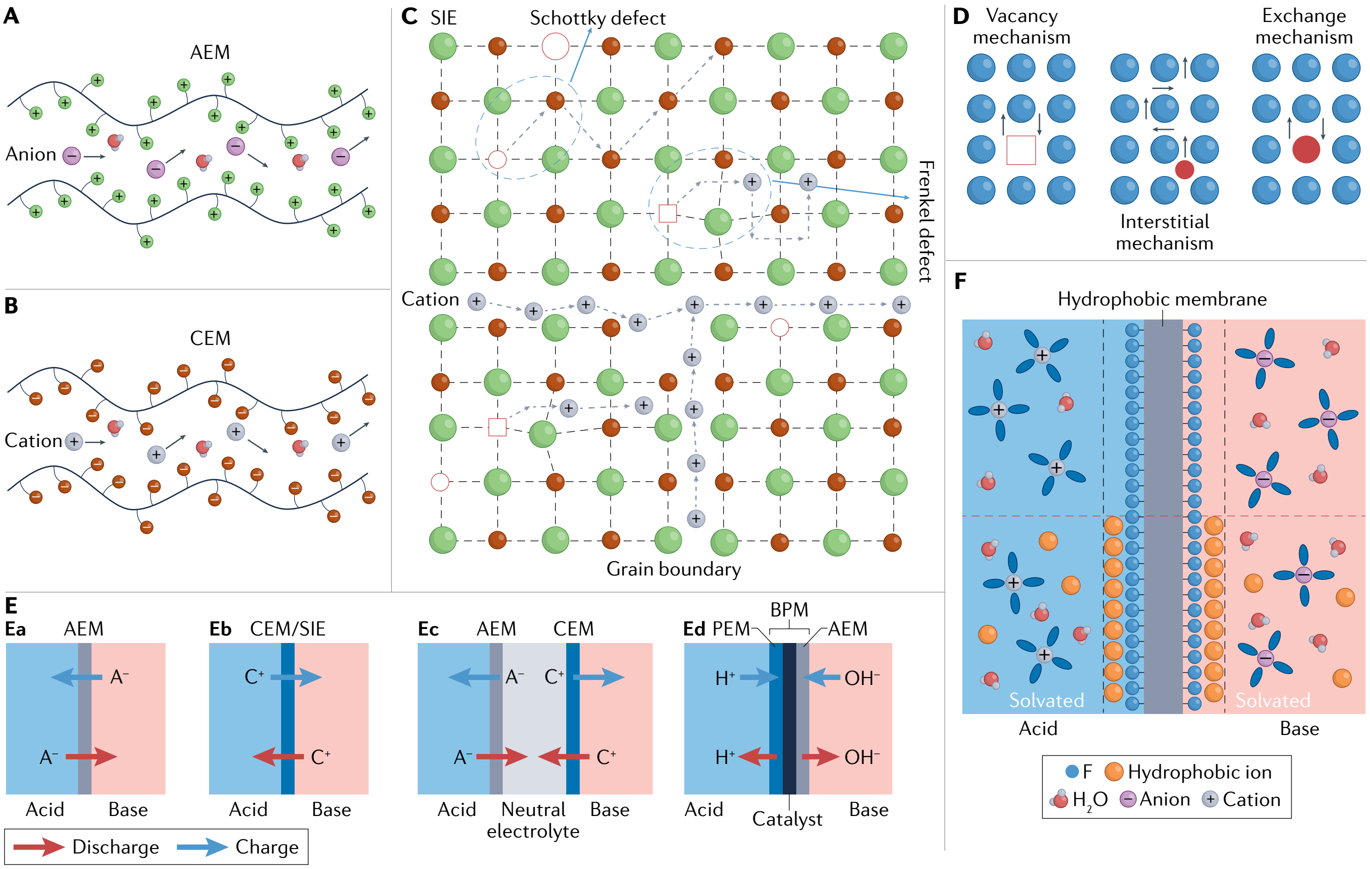

Fig. 2 | **Ion-selective membrane in a decoupled battery. A–C** | Ion-transport mechanisms in an anion-exchange membrane (AEM) (panel **A**), a cation-exchange membrane (CEM) (panel **B**) and a solid inorganic electrolyte (SIE) membrane (panel **C**). The green and brown circles in panels **A** and **B** represent cationic groups and anionic groups, respectively. The frameworks made up of green and orange circles in panel **C** represent the crystal lattice of SIE. Schottky defect, a point defect that is a vacancy in a crystal lattice created by the removal of an atom from the interior to the surface of the crystal; Frenkel defect, a crystal defect that is a combination of a vacancy and an interstitial atom caused by the removal of an atom from the lattice to the interstitial position. **D** | The specific ion diffusion mechanisms in SIE. The red box, orange circles and blue circles stand for vacancy, interstitial atoms and matrix atoms, respectively. **E** | Four typical configurations for membranes in a decoupled battery. **F** | A hydrophobic membrane can selectively adsorb and transport hydroponic ions, the purple anions and grey cations in panel **F** refer in particular to OH^- and H^+, respectively; other ions are not shown here. A^-, anion; BPM, bipolar membrane; C^-, cation; PEM, proton-exchange membrane.

Bipolar membranes (BPMs). A special class of ion-exchange membranes constituted by a cation-exchange and an anion-exchange layer, which allows the generation of protons and hydroxide ions via a water dissociation mechanism.

Proton-exchange membrane (PEM). A kind of semipermeable membrane generally made from ionomers and designed to conduct protons.

mainly contain the vacancy mechanism, interstitial mechanism, interstitial-substitutional exchange mechanism and so on[28] (FIG. 2D). Although SIEs are characterized by a higher ion selectivity when compared with IEMs, they may suffer from serious degradation in strong acidic or alkaline environments.

Besides the single-membrane configuration (FIG. 2Ea,Eb), other membranes used in decoupled batteries are the double-membranes configuration (AEM‖CEM, where ‖ represents a double membrane)[12,29] and bipolar membranes (BPMs)[17,30]. In AEM‖CEM, AEM and CEM are separated by a neutral electrolyte, in which the AEM transports specific anions like SO_4^{2-} between the acidic electrolyte and the neutral electrolyte, and the CEM transports specific cations between the alkaline electrolyte and the neutral electrolyte, such as alkali metal ions[12] (FIG. 2Ec). AEM‖CEM can potentially suppress the chemical crossover more efficiently, given that the buffered neutral electrolyte further isolates the acidic and the alkaline electrolytes. Unlike the configurations of AEM‖CEM, BPMs are mainly composed of a proton-exchange membrane (PEM) and an AEM, in between which a catalyst layer promotes the dissociation of water. BPMs enable the dissociation/generation of H_2O and the transport of H^+ and OH^- through the PEM and the AEM, respectively[17] (FIG. 2Ed). The introduction of BPMs in the decoupled battery can make up for the consumption of H^+ and OH^- in catholyte and anolyte, respectively, because either H^+ or OH^- always participates in the electrode reactions. Importantly though, the ionization of water will consume part of the energy derived from the battery reaction upon the discharge process, which will decrease the output voltage of the battery[31]. Compared with the single membrane, AEM‖CEM and BPMs provide more liquid-phase interfaces, which alleviate the neutralization reaction more efficiently. Theoretically, the isolation effects for pH-decoupling electrolytes can enhance and the ion diffusion resistance can also increase by increasing the number of IEMs. Therefore, more IEMs inevitably catch higher overpotential.

Although the multiple-IEMs strategies are able to alleviate the issues that decoupled batteries face, the fundamental challenges to prevent the chemical crossover of pH-decoupling electrolytes — that is, H^+ in acidic catholyte or OH^- in alkaline anolyte diffuses across the IEMs from one side to another side — remain insurmountable due to the limited ionic permselectivity of IEMs. Therefore, upon cycling in most reported decoupled batteries, the pH of acidic catholyte increases and the pH of alkaline anolyte decreases, which subsequently narrow the operating voltage windows of pH-decoupling electrolytes. Furthermore, as many redox reactions are highly dependent on the pH of electrolytes, the pH changes probably deteriorate the performance of decoupled batteries, leading to a low energy density and short lifespan. Theoretically, ion conduction through a compact non-porous membrane is generally categorized into two successive steps, including ion adsorption on the membrane surface and ion diffusion through the membrane matrix[32]. Therefore, blocking either adsorption or diffusion of ions like H^+ and OH^- will cut off their conduction. Both H^+ and OH^- are hydrophilic ions, existing in the aqueous electrolyte as hydrated ions. The hydrophobic membranes with a hydrophobic surface can repulse the adsorption of hydrated ions and only selectively transport hydrophobic ions like $TFSI^-$ and trifluoromethanesulfonate (OTF^-) anions (FIG. 2F), thus stopping the transportation of H^+ and OH^- across the membrane. To this end, hydrophobic membranes should be able to prevent the chemical crossover between acidic catholyte and alkaline anolyte, and, in the near future, a well-designed hydrophobic membrane could afford the decoupled battery with a long cycle life.

In such a decoupled battery, the diffusion of the ions is simultaneously controlled by the electrical potential and the concentration gradient of the electrolytes. The different concentrations of electrolytes on both sides of the ISMs would generate liquid junction potential, which increases almost linearly with the natural logarithm of the electrolyte concentration gradient between the two reservoirs[19,33] (FIG. 3A). As a result, the output or input voltage of the battery (V) is equal to the sum of the battery potential (V_{EC}) and the liquid junction potential (E_j):

$$V = V_{EC} + E_j$$

In a cation-conduction system (FIG. 3Ba,Bb), when the direction of the electric field is in accordance with that of the concentration gradient, the liquid junction potential promotes the diffusion of ions inside the battery, resulting in the increase of discharge voltage or the decrease of charge voltage (FIG. 3Ba,Bb). Otherwise, the liquid junction potential will decrease the discharge voltage or increase the charge voltage (FIG. 3Ba,Bb). However, owing to the opposite moving directions of anions and cations in the same electric field, the final conclusions in the anion-conduction system are just contrary to that in the cation-conduction system (FIG. 3Bc,Bd).

Competitive redox couples

In conventionally developed aqueous battery configurations, such as zinc-manganese dioxide (Zn-MnO_2)[34], nickel-metal hydride (Ni-MH)[35] and nickel-cadmium (Ni-Cd) batteries[36], the cathode and anode are generally separated by a porous membrane, which allows the liquid electrolyte to shuttle through. Under this cell configuration, the electrode materials must be solid, rather than liquid or gas, to prevent chemical crossover between cathode and anode. This requirement exists despite the fact that many low-cost and abundant materials, either in the liquid or the gas phase, are also considered as the promising electrode materials for aqueous batteries. In contrast to the limited materials that can be used in conventional aqueous batteries, any type of material with high electrochemical capacity and appropriate voltage can be used in decoupled batteries. This is possible because the ISMs can prevent the acid–base neutralization reaction between catholyte and anolyte, as well as the chemical crossover of liquid or gaseous materials. Notably, each electrode material has different reaction mechanisms, and should be coupled with different electrode structures as well. An integrated, in-depth understanding of the intricacies of the reaction

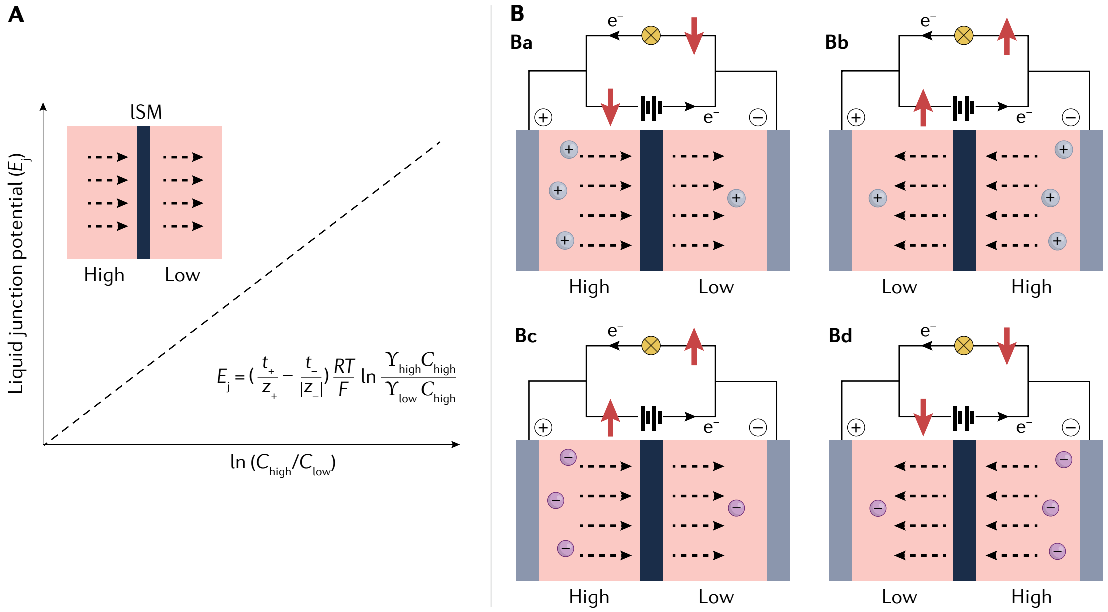

Fig. 3 | **Liquid junction potential in a decoupled battery.** **A** | The liquid junction potentials as a function of the salt concentration gradient[19]. Inset: diagram of ion diffusion across the ion-selective membrane (ISM) driven by a salt concentration gradient. **B** | The liquid junction potentials in decoupled batteries for cation-conduction systems (panels **Ba**, **Bb**) and anion-conduction systems (panels **Bc**, **Bd**). The grey circles represent cations, and the purple circles represent anions. The arrows represent the direction of the salt concentration gradient. γ, activity coefficient; C, salt concentration; C_{high}/C_{low}, salt concentration gradient; E_j, the liquid junction potential; F, Faraday constant; R, gas constant; T, temperature; t_-, transference number for anion; t_+, transference number for cation; z_-, ion valence for anion; z_+, ion valence for cation.

mechanisms for solid, liquid and gas phases is required to achieve the superior capacity, high voltage and excellent electrochemical stability of decoupled batteries.

The electrode reactions for solid electrode materials take place either inside the bulk materials or at the electrode–electrolyte interface by a faradaic or non-faradaic behaviour[37–41]. Correspondingly, charge-storage mechanisms can be classified as: surface adsorption/desorption[37] (FIG. 4Aa); surface redox[38] (FIG. 4Ab); ion insertion/extraction reactions[39] by a rocking-chair mechanism (FIG. 4Ac); or solid–liquid phase transition reactions[40] by oxidation/reduction of charge carriers (FIG. 4Ad). The surface adsorption/desorption reaction, the so-called electrical double-layer capacitors process, only stores charges through surface-controlled ion adsorption and does not involve faradaic reactions[37]. The other three mechanisms that involve pseudocapacitive materials, insertion-type materials and electrolysis-type materials are essentially faradaic processes; they obey Faraday's law and undergo charge-transfer reactions at the electrochemical interface[38]. Notably, the pseudocapacitive materials show a different mechanism (FIG. 4Ab) compared with capacitive charge storage, which involves surface-controlled and faradaic reactions, exhibiting comparable rates but higher energy density to those of double-layer formations in electrical double-layer capacitors[37]. Unlike the capacitive (FIG. 4Aa) and pseudocapacitive materials (FIG. 4Ab) with surface-controlled reactions, the insertion-type materials (FIG. 4Ac) store charges throughout the bulk of the active materials, wherein the diffusion-limited and faradaic reactions occur. Although the insertion-type materials demonstrate high energy density, the diffusion-limited redox reactions are always featured by low power density owing to their sluggish diffusion kinetics[41]. Similar to the pseudocapacitive material, electrolysis-type materials store charges through surface-controlled and faradaic reactions, but through another method of oxidation/reduction of charge carriers[40]. Electrolysis-type materials (FIG. 4Ad) undergo a solid–liquid phase transition via plating/stripping reaction, exhibiting a flat working voltage plateau and an ultra-high capacity, such as with a metal anode[42] or manganese dioxide in the acidic electrolyte[12]. Generally, the solid materials are reduced down in size to the micrometre or even the nanometre scale[43] to improve mass transfer efficiency, and these are mixed with the conductive agent and binder to form a composite electrode on metal foil (FIG. 4B). Certainly, some materials with good conductivity, such as carbon and metal materials, can be fabricated as a binder-free electrode[44] or directly used as an electrode[45] without further treatments.

Almost all liquid electrode materials undergo a surface-controlled and faradaic reaction to store energy in liquid phase[46–48] (FIG. 4Ae). Compared with solid electrode materials, the liquid-phase materials dissolved in electrolyte solutions provide better stability and longer cycle life, because the liquid-phase reaction does not block or swell the electrode. Additionally, the liquid materials theoretically enable faster redox kinetics and higher power density than that of solid materials with the insertion/extraction mechanism, because the ion diffusion rate in liquid electrolytes is typically around several orders of magnitude higher than that in solids[49]. However, the actual reaction kinetics of the liquid materials are limited by the specific surface area

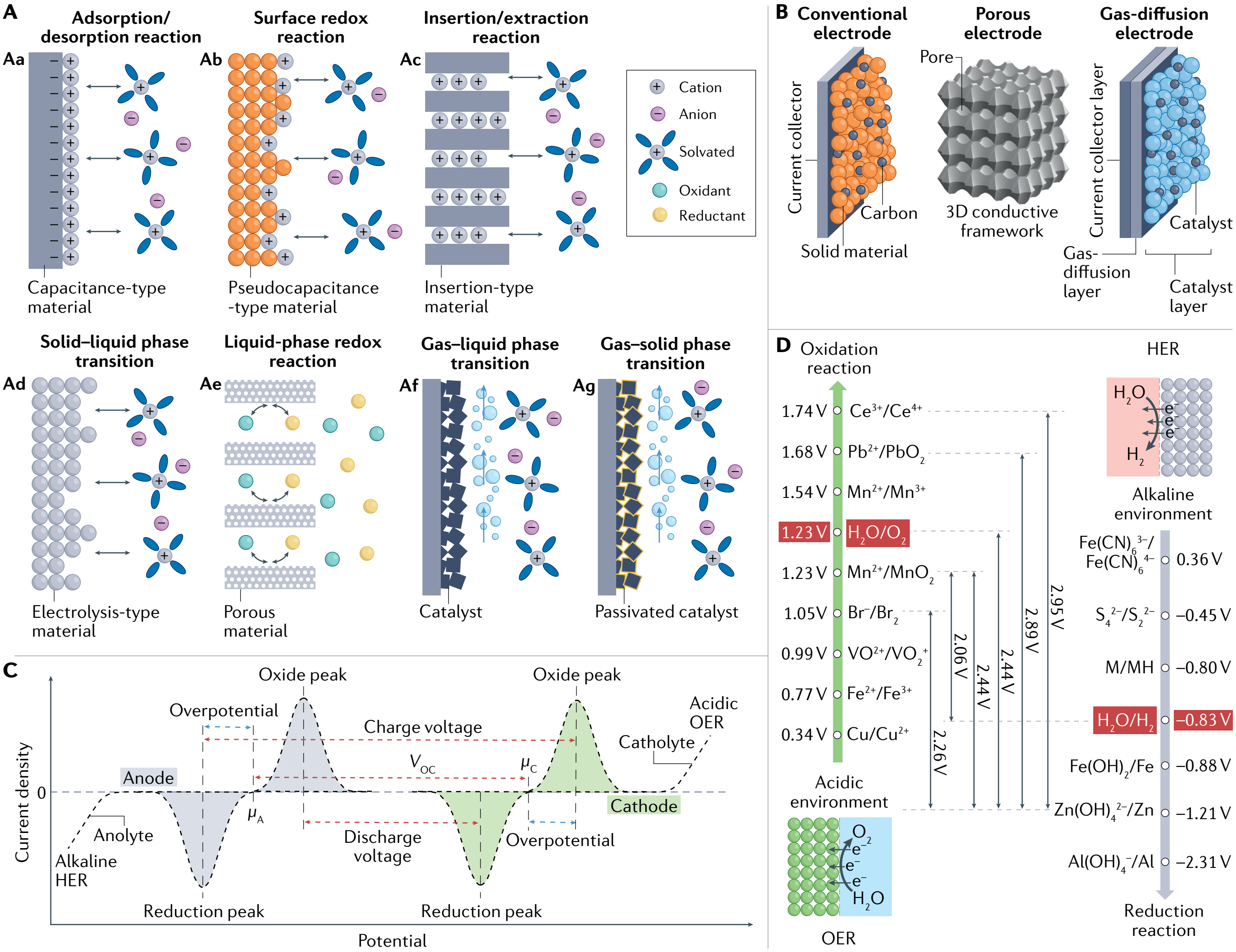

Fig. 4 | **Redox couples in a decoupled battery. A** | Charge-storage mechanisms for solid, liquid and gas materials, including capacitance reaction (panel **Aa**), pseudocapacitance reaction (panel **Ab**), insertion/extraction reaction (panel **Ac**), plating/stripping reaction (panel **Ad**), liquid-phase transition reaction (panel **Ae**), gas–liquid phase transition reaction (panel **Af**) and gas–solid phase transition reaction (panel **Ag**). **B** | Electrode configurations for solid, liquid and gas materials. **C** | Current–voltage profile of cathode, anode and electrolytes. **D** | Summary of standard redox potentials for various redox pairs in acidic and alkaline environments. All the potentials are relative to the standard hydrogen electrode. μ_A, anode electrochemical potential; μ_C, cathode electrochemical potential; HER, hydrogen evolution reaction; OER, oxygen evolution reaction; V_{oc}, open-circuit voltage.

of the electrodes. The liquid-phase reactions are, thus, always equipped with porous electrodes to enable rapid transport of electrons to promote the fast redox reactions in liquid medium[50] (FIG. 4B). The energy density of liquid-phase reactions depends on the solubility of liquid materials. As a result of the limited solubility in aqueous solutions, most of the liquid materials deliver inferior energy densities compared with those of solid materials, which makes them less attractive, especially for use in high-energy-demand energy-storage devices.

Among all types of electrode materials, the gas materials usually have the lowest molecular weights and can undergo multiple electron transfer reactions, thereby, providing the highest energy density[51–53]. However, the gas materials are also characterized by a large overpotential related to the sluggish reaction kinetics. To overcome the huge energy barrier of gas-phase reactions in aqueous batteries, various catalysts are engaged in breaking the covalent bond of gas molecules through a lower-energy mechanism[54]. The gas-phase reactions occur at the solid–liquid–gas (three-phase) interface formed by the gas, electrode and electrolyte, which must simultaneously manage the transport of electrons, water and gas reactants at the electrode[55] (FIG. 4Af,Ag). The gas-diffusion electrodes mainly consist of the gas diffusion layer, the current collector layer and the catalyst layer (FIG. 4B), which are used to mediate these critical processes[56,57]. In a gas-phase reaction, gaseous starting materials are usually converted into liquid or solid products[58,59]. The liquid products dissolve into the electrolyte without passivating the electrode[58] (FIG. 4Af). As a consequence, the non-passivated electrode maintains high activity in subsequent reactions, providing a capacity without degeneration. By contrast, the solid product will cover the electrode surface (FIG. 4Ag) and then physically clog the porous air cathode and chemically deactivate the catalyst, leading to an inferior capacity and unstable cycle performance[59].

The voltage of a decoupled battery depends on the compatibility among the anode, cathode and aqueous electrolyte[60,61]. Specifically, the difference in chemical potential between the cathode (μ_C) and anode (μ_A) is termed as the open-circuit voltage (V_{OC}), which is limited by the operating voltage window of the electrolyte (FIG. 4C). That is, the suitable electrode of the decoupled battery must follow the principle that the μ_C of the cathode lies below the potential of acidic OER and the μ_A of the anode is located above the potential of alkaline HER. Otherwise, the aqueous electrolyte will be split into H_2 and O_2 gas at the anode and cathode sides, respectively. In general, both working voltages of the anode or the cathode are deviated from the chemical equilibrium potential (μ_A or μ_C) owing to the sluggish reaction kinetics for most of the electrode materials in aqueous electrolytes. These deviations enable the generation of an overpotential whether in the charge or the discharge process (FIG. 4C). As a result, V_{OC} is greater than the discharge voltage but less than the charge voltage (FIG. 4C), such that the energy efficiency of the battery must be below 100%. From the perspective of reaction mechanisms, introducing redox couples that show fast reaction kinetics, such as non-diffusion-limited surface redox reaction, presents a feasible approach to improve the energy efficiency of decoupled batteries.

The decoupling-electrolyte strategy expands the operating voltage window of the aqueous electrolyte beyond 3.0 V, thus providing a new platform to develop high-voltage aqueous batteries by coupling various cathode and anode materials (FIG. 4D). To build high-voltage aqueous batteries, desired candidates of the redox couples should exhibit high potential for the cathode in the acidic electrolyte, such as Ce^{4+}/Ce^{3+} (1.74 V versus standard hydrogen electrode (SHE)), PbO_2/Pb^{2+} (1.68 V versus SHE), O_2/H_2O (1.23 V versus SHE), MnO_2/Mn^{2+} (1.23 V versus SHE) and Br^-/Br_2 (1.05 V versus SHE); and low potential for the anode in the alkaline electrolyte, such as H_2O/H_2 (−0.83 V versus SHE), $Fe(OH)_2/Fe$ (−0.88 V versus SHE), $Zn(OH)_4^{2-}/Zn$ (−1.21 V versus SHE) and $Al(OH)_4^-/Al$ (−2.31 V versus SHE). Notably, although the potential of some redox couples, such as Ce^{4+}/Ce^{3+}, PbO_2/Pb^{2+} and Mn^{3+}/Mn^{2+} in the acidic electrolyte or $Fe(OH)_2/Fe$ and $Zn(OH)_4^{2-}/Zn$ in the alkaline electrolyte, exceed the theoretical operating voltage window of pH-decoupling electrolyte, the corresponding redox reactions still occur in decoupled batteries on the cathode or anode side because their fast kinetics suppress the OER or the HER[62]. Recently, various decoupled batteries combined with competitive redox couples have been generated and their feasibility has been evaluated in the real energy-storage systems (TABLE 1). It should be noted that some decoupled batteries deliver voltages exceeding their theoretical voltages, which is probably attributed to the liquid junction potential discussed above[12]. Considering the comprehensive perspectives of voltage, energy density and feasibility, cost and environment, we mainly discuss three decoupled battery prototypes, including decoupled Zn–MnO_2, Zn–Br and Zn–air batteries here.

Decoupled battery prototypes

Decoupled Zn–MnO_2 battery. Traditional alkaline Zn–MnO_2 batteries are composed of MnO_2, a proton insertion cathode and a Zn anode of the solution type[63,64]. In a strong basic environment, the reduction of MnO_2 can be classified into two successive stages[65] (FIG. 5a). In stage 1, protons from water molecules are inserted into the MnO_2 structure to form MnOOH, causing the reduction of Mn^{4+} to Mn^{3+} with a capacity of 308 mAh g^{-1}. Subsequently, the generated MnOOH in the first stage involves a dissolution reaction that releases Mn^{3+} to the electrolyte. These Mn^{3+} species are then further reduced on the electrode surface to form insoluble $Mn(OH)_2$ at the end of the discharge process. The second stage covers the composition range from MnOOH to $Mn(OH)_2$, exhibiting another capacity of 308 mAh g^{-1} by a dissolution–precipitation mechanism (FIG. 5a). However, owing to the poor reversibility of stage 2, the alkaline Zn–MnO_2 batteries are still only employed as the primary battery. Limiting the depth of discharge state of alkaline Zn–MnO_2 batteries to stay at stage 1, the batteries are rechargeable[66] but at the expense of the energy density (theoretical voltage: 1.5 V; theoretical capacity: ~176 mAh g^{-1} based on the total mass of cathode and anode). Even so, the alkaline Zn–MnO_2 second batteries still exhibit inferior cycle lifespan, due to the formation of mixed Zn–Mn oxide phases upon discharge, which are hardly decomposed[63].

Unlike the complex reduction process in alkaline solution, MnO_2 can reversibly dissolve in a strong acidic electrolyte with two-electron transfer[12,17], achieving superior specific capacity (616 mAh g–^{1}) and voltage (1.23 V versus SHE) with a redox pair of MnO_2/Mn^{2+}. Therefore, a decoupled Zn–MnO_2 battery with a pH-decoupling electrolyte has been generated recently (FIG. 5b). This hybrid battery is composed of a cathodic tank that contains a Mn^{2+}-based acidic catholyte and an anodic tank with a Zn^{2+}-based alkaline anolyte, and an ISM to isolate each of these two tanks. In these hybrid batteries, both MnO_2 and Zn electrode reactions follow the plating/stripping mechanism by oxidation/reduction charge carriers of Mn^{2+} and Zn^{2+} ions, respectively. Benefiting from the high voltage and capacity of the MnO_2/Mn^{2+}, the decoupled Zn–MnO_2 batteries possess a high theoretical voltage of 2.44 V and capacity of ~352 mAh g^{-1} (based on the total mass of cathode and anode). Both AEM||CEM[12] and BPM[17] have been tested as separators in these decoupled Zn–MnO_2 batteries. Two early examples of cell systems presented in 2020 are MnO_2|acidic electrolyte|AEM|neutral electrolyte|CEM|alkaline electrolyte|Zn and MnO_2|acidic electrolyte|BPM|alkaline electrolyte|Zn (| represents the phase separation between the electrode and the electrolyte or the membrane and the electrolyte), both of which deliver voltages approaching or even exceeding their theoretical potential (a part of the voltage is contributed by liquid junction potential).

Table 1 | **Comparison of different decoupled aqueous batteries**

Battery type	Electrochemical reaction mechanism	Membrane	Theoretical voltage (V)	Working voltage (V)	Characteristics	Ref.
Redox flow	$+: Ce_2O^{6+} + 2H^+ + 2e^- \rightleftharpoons 2Ce^{3+} + H_2O$ $-: Zn + 4OH^- \rightleftharpoons Zn(OH)_4^{2-} + 2e^-$	AEM + CEM	3.08	~2.8	High energy density Flexibility Complex manufacture	16
Redox flow	$+: Br_2 + 2e^- \rightleftharpoons 2Br^-$ $-: Zn + 4OH^- \rightleftharpoons Zn(OH)_4^{2-} + 2e^-$	BPM	2.26	~2.1	High energy density Flexibility Complex manufacture	30
Redox flow	$+: Fe^{3+} + e^- \rightleftharpoons Fe^{2+}$ $-: Zn + 4OH^- \rightleftharpoons Zn(OH)_4^{2-} + 2e^-$	AEM + CEM	1.99	~1.8	Limited energy density Flexibility Complex manufacture	96
Zn–MnO_2	$+: MnO_2 + 4H^- + 2e^- \rightleftharpoons Mn^{2+} + 2H_2O$ $-: Zn + 4OH^- \rightleftharpoons Zn(OH)_4^{2-} + 2e^-$	BPM	2.44	~2.44	High energy density High power density Complex manufacture	17
MH–MnO_2	$+: MnO_2 + 4H^- + 2e^- \rightleftharpoons Mn^{2+} + 2H_2O$ $-: 2MH + 2OH^- \rightleftharpoons 2M + 2H_2O + 2e^-$	CEM	2.03	~2.20	Low power density Memory effect	21
Zn–PbO_2	$+: PbO_2 + 2e^- + 4H^+ + SO_4^{2-} \rightleftharpoons PbSO_4 + 2H_2O$ $-: Zn + 4OH^- \rightleftharpoons Zn(OH)_4^{2-} + 2e^-$	AEM + CEM	2.89	~2.95	High energy density Severe side reaction Environmental issue Complex manufacture	68
MH–PbO_2	$+: PbO_2 + 2e^- + 4H^+ + SO_4^{2-} \rightleftharpoons PbSO_4 + 2H_2O$ $-: 2MH_x + 2OH^- \rightleftharpoons 2MH_{x-1} + 2H_2O + 2e^-$	AEM + CEM	2.48	~2.10	Environmental issue Complex manufacture Memory effect	97
Metal–air	$+: O_2 + 4H^+ + 4e^- \rightleftharpoons 2H_2O$ $-: Zn + 4OH^- \rightleftharpoons Zn(OH)_4^{2-} + 2e^-$	SIE	2.44	~1.92	High energy density Low energy efficiency Severe side reaction	25
Metal–air	$+: O_2 + 4H^+ + 4e^- \rightleftharpoons 2H_2O$ $-: Fe + 2OH^- \rightleftharpoons Fe(OH)_2 + 2e^-$	SIE	2.11	~1.60	Low energy density Low energy efficiency	90
Metal–air	$+: O_2 + 4H^+ + 4e^- \rightarrow 2H_2O$ $-: Al + 4OH^- \rightarrow Al(OH)_4^- + 3e^-$	AEM	3.54	~2.56	High energy density Low energy efficiency Severe side reaction	91

Under the electrochemical reaction mechanisms, + and – stand for cathode reaction and anode reaction, respectively. AEM, anion-exchange membrane; BPM, bipolar membrane; CEM, cation-exchange membrane; SIE, solid inorganic electrolyte.

The main challenge associated with decoupled Zn–MnO_2 batteries is the poor conductivity of MnO_2. Theoretically, the deposition weights of charge/discharge products are highly dependent on their conductivity. Owing to the poor conductivity, only a thin layer of MnO_2 can be plated on the surface of conductive substrates during the charging process, which leads to a low mass loading of active materials. The plated MnO_2 is also unable to be fully utilized upon the subsequent discharge process, because the inner layer of MnO_2 that is directly contacted with the conductive substrates will be dissolved first. The dissolution of this inner layer of MnO_2 then causes the outer layer of MnO_2 to exfoliate from the electrode. Therefore, to date, decoupled Zn–MnO_2 batteries have shown unsatisfied real capacity and low energy density, especially in the fast charge/discharge process. A recent study demonstrates that such issues can be avoided by a 3D array electrode, thus allowing a high MnO_2 loading to be used to develop a more practical, high-specific-energy Zn–MnO_2 battery[67].

Similar to the MnO_2 cathode, the PbO_2 cathode also undergoes a two-electron transfer reaction in acidic electrolyte with a theoretical voltage of ~1.68 V versus SHE and a theoretical capacity of ~224 mAh g^{-1}. Recently, a decoupled Zn–PbO_2 battery was generated by simply coupling an acidic PbO_2 cathode with an alkaline Zn anode[68], affording a high theoretical energy density of ~509 Wh kg^{-1} (based on the total mass of PbO_2 and Zn). However, using such lead-contained batteries will damage the environment if they are handled improperly. Consequently, the decoupled Zn–PbO_2 batteries can hardly be applied to future electrical energy-storage systems or electric vehicles, which require batteries that are environmentally friendly and safe.

Decoupled Zn–Br battery. The Zn–Br battery consists of a solid Zn anode and a liquid Br_2 cathode in a $ZnBr_2$ aqueous electrolyte, which was first patented in 1885 and was developed as a hybrid flow battery in the 1970s[69,70]. The battery reaction contains the reduction of Br_2 or oxidation of Br^- on the cathode sides and the stripping/plating of Zn onto the anode side, exhibiting a theoretical cell voltage of ~1.8 V. Although the liquid Br_2 cathode provides a relatively high potential (1.05 V versus SHE), fast redox kinetics and excellent stability[71,72], the low potential of the redox pair of Zn^{2+}/Zn (−0.74 V versus SHE) limits the working voltage of a Zn–Br battery and devalues its potential application in practical devices. Recently, an alternative decoupled Zn–Br battery was developed by simply changing the anolyte from a neutral one to an alkaline one[30] (FIG. 5c). Owing to the more negative potential (−1.21 V versus SHE) of the $Zn(OH)_4^{2-}/Zn$ redox pair that occurs in alkaline electrolytes, this decoupled Zn–Br battery achieves an actual output voltage of ~2.1 V (close to the theoretical voltage of ~2.26 V), a high reversible discharge capacity of 395 mAh g^{-1} and a long-term lifespan of up to 2,000 cycles[30]. Therefore, the decoupled Zn–Br batteries are considered as the most promising candidates for use in large-scale energy-storage systems. However, due to the volatility and corrosivity of the Br_2 cathode, the practical applications of the decoupled Zn–Br batteries are confronted with potential safety and environmental concerns.

Generally, Br_2 is hardly soluble in water, but it can complex with Br^- ion to form highly soluble polybromide anion (Br_{2n+1}^-)[73,74]. Nevertheless, both Br_2 and its Br_{2n+1}^- form are easily volatile even at ambient temperature[75], limiting the concentration of the active materials in the catholyte and raising serious safety and environmental concerns. Organic quaternary ammonium cation compounds, so-called bromine complexing agents (BCAs), can convert polybromides into a less volatile form to stabilize them[76–78]. Specifically, the highly soluble BCAs are complexed with polybromide to form

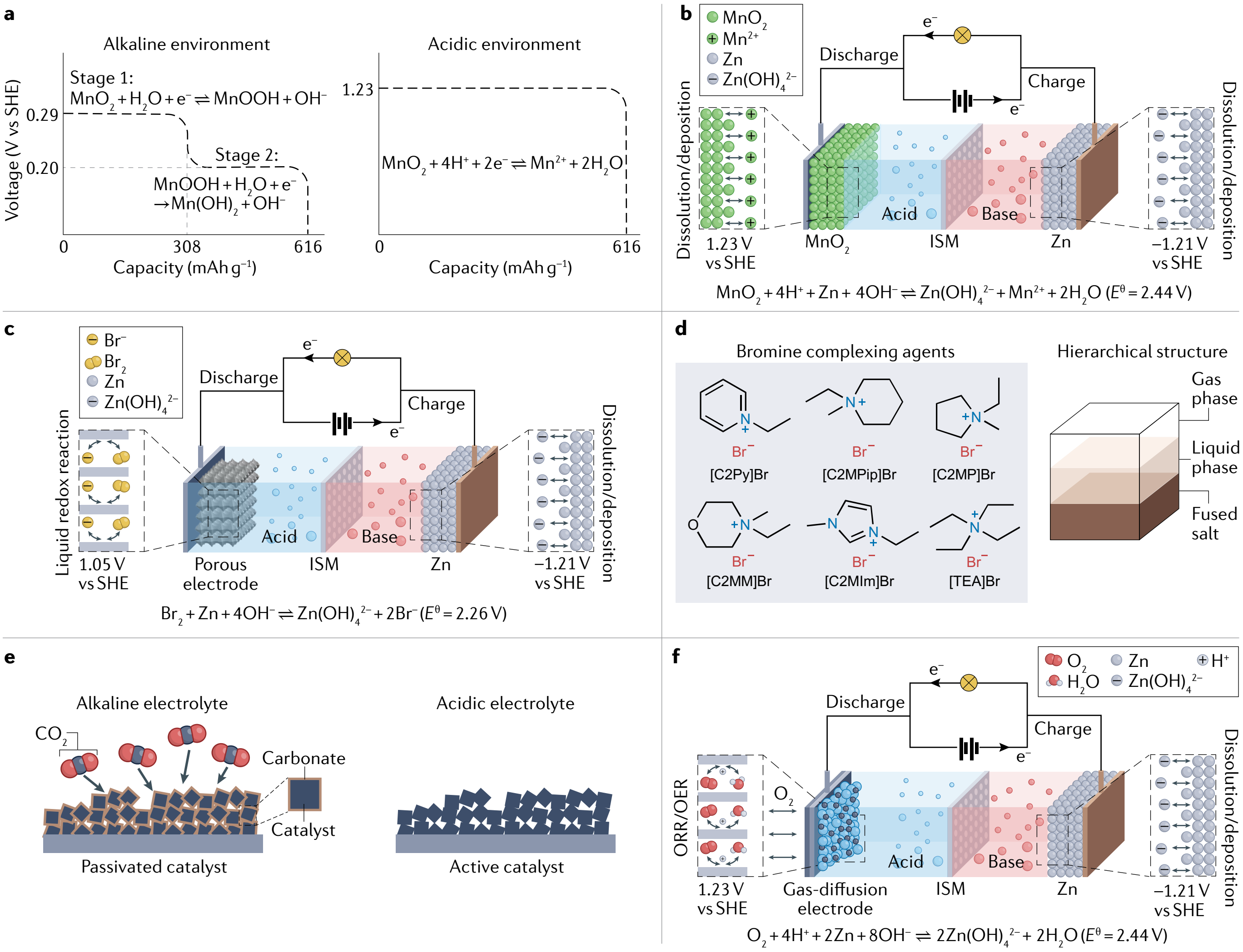

Fig. 5 | **Decoupled battery prototypes. a** | The theoretical discharge profiles of MnO_2 in alkaline and acidic electrolytes. **b** | Decoupled Zn–MnO_2 battery with a solid MnO_2 in acidic catholyte and solid Zn metal in alkaline anolyte. **c** | Decoupled Zn–Br battery with a liquid Br_2 cathode and solid Zn metal in alkaline anolyte. **d** | The typical six building blocks for bromine complexing agents and the hierarchical structure of aqueous Br_2 electrolyte with bromine complexing agents. **e** | Different morphological characteristics for air-cathode catalysts in alkaline and acidic electrolytes. **f** | A decoupled Zn–air battery with a gas cathode in acidic catholyte and solid Zn metal in alkaline anolyte. [C2MIm]Br, 1-ethyl-3-methylimidazol-1-iumbromide; [C2MM]Br, 1-ethyl-1-methylmorpholin-1-iumbromide; [C2MP]Br, 1-ethyl-1-methylpyrrolidin-1-iumbromide; [C2MPip]Br, 1-ethyl-1-methylpiperidinbromide; [C2Py]Br, 1-ethylpyridin-1-iumbromide; ISM, ion-selective membrane; OER, oxygen evolution reaction; ORR, oxygen reduction reaction; SHE, standard hydrogen electrode; [TEA]Br, tetraethylammoniumbromide.

a less soluble or insoluble product in aqueous media, thus enabling the Br_2 solution to generate a heavy second phase in solution[76,79] (FIG. 5d). This heavy phase is commonly known as the fused salt phase, which allows for a highly concentrated Br_2 catholyte and reduces the Br_2 vapour pressure in the gas-phase layer (FIG. 5d). Consequently, the BCAs are expected to stimulate the development of high-security and high-energy-density decoupled Zn–Br batteries.

Decoupled Zn–air battery. Zn–air batteries represent one of the most viable future options for powering electric vehicles owing to their potential low cost, good safety and high energy density. The typical configuration of Zn–air batteries consists of a porous carbonaceous air cathode loaded with a noble metal catalyst and a metal Zn anode in alkaline aqueous electrolytes[80–82]. During discharge, O_2 from the air reacts with H_2O to form OH^- at the cathode side, and the generated OH^- migrate to the anode side and react with metal zinc to produce zincate $[Zn(OH)_4^{2-}]$. Upon charging, reverse processes occur on the cathode and anode sides, respectively. Based on the Nernst equation, the theoretical voltage of Zn–air batteries is calculated to be 1.65 V, while almost all practical devices deliver a voltage less than 1.4 V (even after optimization)[81,83]. Generally, 6–7 M KOH alkaline electrolytes are used to sustain both optimized ionic conductivity and superior oxygen reduction reaction (ORR)/OER kinetics[84]. However, the side reaction between alkaline electrolytes and CO_2 from air produces insoluble carbonate salts, which irreversibly consumes electrolyte and physically clogs the porous air cathode and chemically deactivates the catalyst[59,82] (FIG. 5e). Using neat O_2 (not air) is expected to prolong the cell life, but it inevitably induces complicated cell designs, increased manufacturing/maintenance costs and substantial underutilization of its theoretical energy density[85].

Theoretically, acidic electrolytes offer the more positive potential for the O_2 redox reaction and simultaneously make the air cathode immune to CO_2 poisoning issues[25] (FIG. 5e). A decoupled Zn–air battery with dual electrolyte, which consists of an alkaline anolyte to support the Zn plating/stripping reaction on the anode side and an acidic catholyte to sustain the OER/ORR on the cathode side, was generated[25,86,87] (FIG. 5f). Benefiting from the advantages of acidic electrolytes, the thermodynamic voltage of the decoupled Zn–air batteries is significantly increased from 1.65 V to 2.44 V, which is higher than that of commercial lead-acid batteries and comparable with lithium titanate batteries. However, this hybrid battery can only provide an output voltage less than 2 V, even at low current density. This unsatisfied electrochemical performance might be induced by the sluggish kinetics of the ORR in the acidic electrolyte[88], which should be circumvented in the near future by novel ORR catalysts with high activity and stability.

In conventional Zn–air batteries, it is common for a bifunctional air electrode to serve as both the ORR and the OER catalyst. However, the OER and ORR have different preferences in terms of active sites and electrochemical reaction environments[89]. Specifically, the ORR prefers hydrophobic sites, which are favourable for gas absorption, while the OER prefers hydrophilic sites to promote gas desorption from the electrode surface[89]. Therefore, it is challenging for a single electrode to achieve high activity for both the OER and the ORR. To this end, ORR and OER electrodes were decoupled recently in a decoupled Zn–air battery[25]. In this cell configuration, a second electrode independent of the ORR electrode is directly loaded with catalyst on a metal mesh, such as nickel, stainless steel and titanium, to serve as an OER electrode. This decoupled design strategy optimizes catalyst activity for the ORR and the OER, but also overcomes carbon corrosion and catalyst dissolution during the OER. Therefore, this novel decoupling strategy is considered an efficient means to improve the energy efficiency and prolong the cycle life of the decoupled Zn–air battery at the present state.

Importantly, other decoupled metal–air batteries (beyond decoupled Zn–air batteries) are able to be designed and fabricated applying the same principle. For instance, decoupled Fe–air[90] and Al–air batteries[91] have been fabricated recently by simply changing the Zn anode with Fe and Al, respectively. Compared with the Zn–air batteries, the decoupled Al–air batteries offer advantages, such as the ultra-high theoretical voltage of 3.54 V and energy density of ~10,550 Wh kg^{-1} (based on the mass of Al). However, the plating of Al metal in an aqueous electrolyte is considered to be impossible, because the potential of $Al(OH)_4^-/Al$ (−2.31 V versus SHE) is far below the theoretical potential of the HER in the alkaline electrolyte (pH = 14). As a result, the decoupled Al–air batteries are not rechargeable. Additionally, the strong alkaline electrolytes are known to corrode Al metal, thus resulting in a high self-discharge rate and causing a low utilization of Al anode.

Summary and outlook

Overall, pH-decoupled electrolytes work beyond widening the operating voltage window of aqueous electrolytes. They also enable the formation of new energy-storage systems from any forms of materials with both high capacity and suitable voltage. Therefore, strategies that use decoupled batteries have great potential to break through the voltage and energy density limitations of aqueous batteries. Encouragingly, significant progress has been made regarding the designs of decoupled batteries in recent years. Implementing decoupled batteries across practical applications will require further research and developments across its components, such as ISMs, electrodes and possible cell configurations.

Next-generation ion-selective membranes. The viability of decoupled batteries hinges on the advancement of ISMs. Generating ISMs with high selectivity, high conductivity and good electrochemical stability requires a comprehensive approach towards experiments and theories, coupled with the use of advanced state-of-the-art characterization techniques to reveal the intricate ion-transport mechanisms. To date, almost all of the ISMs, including IEMs and SIEs, used in decoupled batteries are unable to afford a long cycle life owing to their poor permselectivity or their unstable structure in strong acidic/alkaline solution. There are a couple of

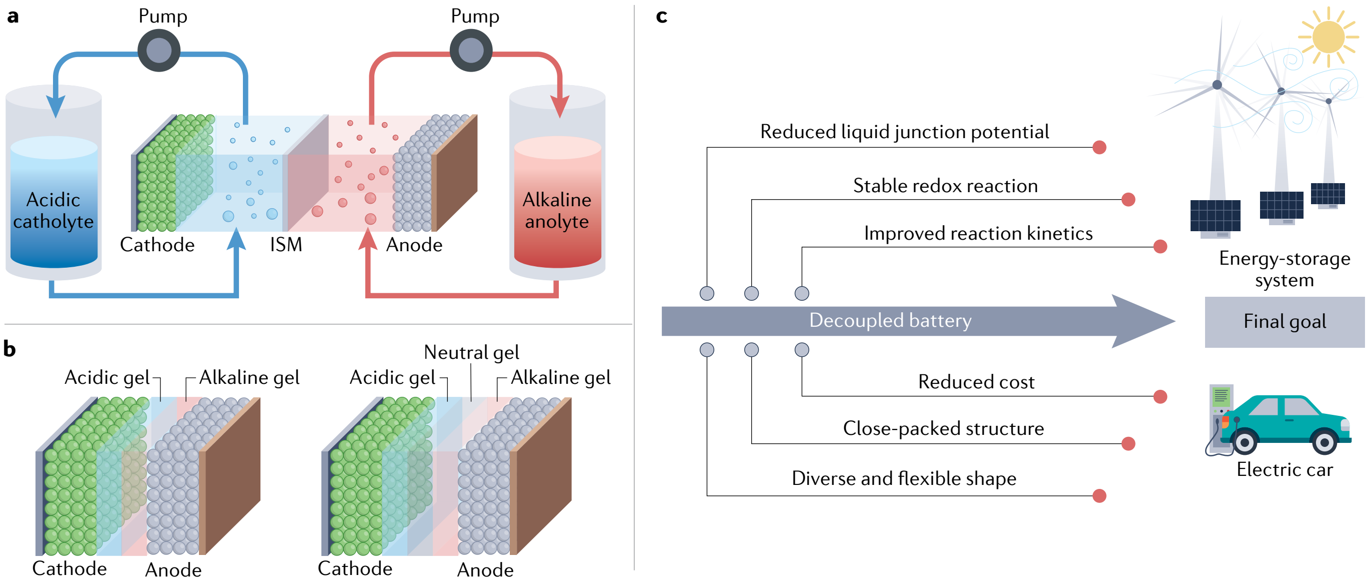

Fig. 6 | **Cell configurations for decoupled batteries in the future. a** | Flow-decoupled battery. **b** | Membrane-free decoupled battery. **c** | The typical characteristics and ultimate application goals for the flow-decoupled battery and membrane-free decoupled battery. ISM, ion-selective membrane.

approaches that sustainably and efficiently inhibit the crossover of hybrid electrolytes. For instance, the ionic permselectivity of IEMs must improve, such as increasing the crosslinking degree of polymer matrix. Or the chemical stability of SIEs in acidic/alkaline solutions can be boosted, improving the corrosion resistance of SIEs by doping or construction of an artificially protective layer to protect SIEs. Another approach is to design tailored ISMs for decoupled batteries. For example, a polymeric single-Zn^{2+}-ion conductor that could only selectively absorb and transport Zn ions was recently generated. Such an ISM prevents the crossover of hybrid electrolytes, making high-performance decoupled metal–air batteries possible[86]. Developing a hydrophobic membrane that selectively transports hydrophobic ions seems to be the most efficient way to overcome the challenges facing decoupled batteries owing to the fact that H^+ and OH^- are hydrophilic. However, the hydrophobic ions, such as $TFSI^-$ and OTF^-, usually possess large sizes — hundreds or even thousands of times larger than that of the proton. It is difficult to transport these huge ions across the hydrophobic membrane via the traditional conduction strategies in a 'vehicular' manner[92]. Like the Grotthuss mechanism for protonic conduction[92], the diffusion-free conductive pathways are expected to enable the hydrophobic ion to be conductible in a hydrophobic membrane.

The use of ISMs in decoupled batteries also captures larger charge-transfer resistance than that of conventional batteries with one electrolyte due to the introduction of additional electrolyte–electrolyte interfaces. The ionic conductivity of current ISMs need to be improved to reduce the overpotential originating from ISMs. However, given that the ionic conductivity and the ionic permselectivity of ISMs are basically opposites of each other, a balance between them is required for an optimal overall ISM performance. Additionally, the large overpotential for most of the reported decoupled batteries mainly arises from the sluggish kinetics of the electrode reaction[25,90]. Therefore, improving the reaction kinetics of redox couples can compensate for the voltage losses caused by ISMs.

Reformative electrode. Strong acid or strong alkaline electrolytes will corrode the electrode, especially the metallic anode in an alkaline environment; electrode protection, therefore, represents one of the core challenges in decoupled aqueous batteries. Many sophisticated strategies for electrode protection strategies in metal–air and metal-ion batteries include electrode architecture designs, electrolyte additives and artificially constructed protective layers. These strategies are expected to be transplanted in decoupled batteries[93,94], promoting the practical application of decoupled batteries in the real world. Currently available ORR/OER catalysts have demonstrated low catalytic activity and insufficient durability in the acidic electrolytes. Consequently, the existing decoupled metal–air batteries show inferior rate capability and unsatisfied lifespan. Fortunately, since ORR/OER catalysts are crucial for many important reactions, including (reversible) PEM fuel cells and (reversible) electrolysers, the activity breakthrough of ORR/OER catalysts in these fields will certainly accelerate their development for decoupled metal–air batteries.

Optimal cell configuration. In most of the decoupled aqueous batteries, H^+ and OH^- participate in electrochemical reactions at the cathode and anode, respectively. For instance, in a decoupled Zn–air battery, H^+ reacts with oxygen to form water during the ORR, which is accompanied by an anode reaction between OH^- and Zn metal. The acidic ORR makes the pH of the catholyte increase; meanwhile, the alkaline Zn oxidation reaction

Grotthuss mechanism
Also known as proton-hopping mechanism, a proton transport mode in the hydrogen-bond network of water molecules or other hydrogen-bonded liquids, which is completed via the cooperative breaking and formation of hydrogen bonds and O–H covalent bonds.

causes a decline in the pH of the anolyte. Since the voltage of the ORR is highly dependent on the pH of the catholyte, the working voltage of decoupled Zn–air batteries drops as the pH increases. Furthermore, the directional transport of the mediator ions through the ISMs causes the electrolyte concentrations to rise on one side and fall on the other, generating a concentration gradient between two electrolytes. Notably, the reverse concentration gradient limits the diffusion of mediator ions, thereby polarizing the cells. Theoretically, increasing the amount or concentration of electrolytes may alleviate the above challenges. However, owing to the lag in electrolyte diffusion, the change of local pH or the local concentration difference at the electrode–electrolyte interface and the electrolyte–electrolyte interface cannot be timely and completely eliminated. Designing appropriate cell structures like the flow cell configurations (FIG. 6a), which maintains an approximate constant electrolyte concentration by facilitating the flow of electrolyte, may be an efficient way to solve the above challenges. Notably, the flow-decoupled batteries are always characterized by their large volume and complex structure, and are, therefore, suitable to be applied in the large-scale energy-storage system rather than the other energy devices that call for batteries with compacted structures and high energy density (FIG. 6c). To expand the application scenarios of decoupled batteries, membrane-free decoupled batteries have been made using self-standing gel electrolytes to replace liquid electrolyte[95]. In such configurations, two or three types of gel electrolyte (acidic gel/alkaline gel or acidic gel/neutral gel/alkaline gel) are closely packed between the cathode and the anode (FIG. 6b), which maintains their respective acidic or alkaline environments, and simultaneously prevent the crossover of hybrid electrolytes. Notably, the membrane-free decoupled batteries simplify the configurations of the static or flow-decoupled battery and avoid the use of expensive IEMs, which are expected to be applicable to electric vehicles due to their potential high energy density, high safety and low cost (FIG. 6c).

Outlook. Despite the fact that decoupled aqueous batteries have attractive theoretical voltages and energy densities, the state-of-the-art decoupled aqueous batteries still cannot guarantee practically appealing performances especially in the terms of lifespan, rate capability and energy efficiency. As the research of decoupled aqueous batteries is in its infant stage, more comprehensive and systematic studies involving interface chemistry, electrochemistry, theoretical calculation, membrane technology and characterization techniques are required to reveal the battery reaction and ionic transport mechanisms, thereby improving battery performance. Importantly, the rise of decoupled aqueous batteries will revolutionize the battery chemistries and provide advanced battery systems with affordable cost, high safety, high energy density and long lifespans for future energy storage.

1. Armand, M. & Tarascon, J. M. Building better batteries. *Nature* **451**, 652–657 (2008).
2. Xu, K. Electrolytes and interphases in Li-ion batteries and beyond. *Chem. Rev.* **114**, 11503–11618 (2014).
3. Pasta, M., Wessells, C. D., Huggins, R. A. & Cui, Y. A high-rate and long cycle life aqueous electrolyte battery for grid-scale energy storage. *Nat. Commun.* **3**, 1149 (2012).
4. Kim, H. et al. Aqueous rechargeable Li and Na ion batteries. *Chem. Rev.* **114**, 11788–11827 (2014).
5. Tripathi, A. M., Su, W. N. & Hwang, B. J. In situ analytical techniques for battery interface analysis. *Chem. Soc. Rev.* **47**, 736–851 (2018).
6. Chao, D. et al. Roadmap for advanced aqueous batteries: from design of materials to applications. *Sci. Adv.* **6**, eaba4098 (2020).
7. Sui, Y. & Ji, X. Anticatalytic strategies to suppress water electrolysis in aqueous batteries. *Chem. Rev.* **121**, 6654–6695 (2021).
8. Suo, L. et al. "Water-in-salt" electrolyte enables high-voltage aqueous lithium-ion chemistries. *Science* **350**, 938–943 (2015).
This paper reports that water-in-salt electrolytes significantly widen the operation voltage windows of aqueous electrolytes and enable high-voltage aqueous LIBs.
9. Yamada, Y., Wang, J., Ko, S., Watanabe, E. & Yamada, A. Advances and issues in developing salt-concentrated battery electrolytes. *Nat. Energy* **4**, 269–280 (2019).
10. Xie, J., Liang, Z. & Lu, Y. C. Molecular crowding electrolytes for high-voltage aqueous batteries. *Nat. Mater.* **19**, 1006–1011 (2020).
This paper reports that molecular crowding agents are able to break the hydrogen-bond network of water, thereby substantially suppressing the activity of water.
11. Bi, H. et al. A universal approach to aqueous energy storage via ultralow-cost electrolyte with super-concentrated sugar as hydrogen-bond-regulated solute. *Adv. Mater.* **32**, 2000074 (2020).
12. Zhong, C. et al. Decoupling electrolytes towards stable and high-energy rechargeable aqueous zinc-manganese dioxide batteries. *Nat. Energy* **5**, 440–449 (2020).
This paper reports a decoupled Zn–MnO_2 battery based on the multiple IEMs, including CEM and AEM.
13. Wang, F. et al. Highly reversible zinc metal anode for aqueous batteries. *Nat. Mater.* **17**, 543–549 (2018).
14. McEldrew, M., Goodwin, Z. A., Kornyshev, A. A. & Bazant, M. Z. Theory of the double layer in water-in-salt electrolytes. *J. Phys. Chem. Lett.* **9**, 5840–5846 (2018).
15. Wang, X., Chandrabose, R. S., Jian, Z., Xing, Z. & Ji, X. A 1.8 V aqueous supercapacitor with a bipolar assembly of ion-exchange membranes as the separator. *J. Electrochem. Soc.* **163**, 1853–1858 (2016).
16. Gu, S., Gong, K., Yan, E. Z. & Yan, Y. A multiple ion-exchange membrane design for redox flow batteries. *Energy Environ. Sci.* **7**, 2986–2998 (2014).
This paper introduces the multiple IEM designs into flow batteries to improve the working voltages of flow batteries.
17. Chao, D. et al. Atomic engineering catalyzed MnO_2 electrolysis kinetics for a hybrid aqueous battery with high power and energy density. *Adv. Mater.* **32**, 2001894 (2020).
18. Logan, B. E. & Elimelech, M. Membrane-based processes for sustainable power generation using water. *Nature* **488**, 313–319 (2012).
19. Liu, X. et al. Power generation by reverse electrodialysis in a single-layer nanoporous membrane made from core–rim polycyclic aromatic hydrocarbons. *Nat. Nanotechnol.* **15**, 307–312 (2020).
20. Yip, N. Y., Brogioli, D., Hamelers, H. V. M. & Nijmeijer, K. Salinity gradients for sustainable energy: primer, progress, and prospects. *Environ. Sci. Technol.* **50**, 12072–12094 (2016).
21. Yang, M., Chen, R., Shen, Y., Zhao, X. & Shen, X. A high-energy aqueous manganese–metal hydride hybrid battery. *Adv. Mater.* **32**, 2001106 (2020).
22. Jin, Z., Li, P. & Xiao, D. A hydrogen-evolving hybrid-electrolyte battery with electrochemical/photoelectrochemical charging from water oxidation. *ChemSusChem* **10**, 483–488 (2017).
23. Ran, J. et al. Ion exchange membranes: new developments and applications. *J. Membr. Sci.* **522**, 267–291 (2017).
24. Luo, T., Abdu, S. & Wessling, M. Selectivity of ion exchange membranes: a review. *J. Membr. Sci.* **555**, 429–454 (2018).
25. Li, L. & Manthiram, A. Long-life, high-voltage acidic Zn–air batteries. *Adv. Energy Mater.* **6**, 1502054 (2016).
This paper reports a decoupled Zn–air battery based on a NASICON-type Li-ion solid electrolyte.
26. Chen, L., Guo, Z., Xia, Y. & Wang, Y. High-voltage aqueous battery approaching 3 V using an acidic–alkaline double electrolyte. *Chem. Commun.* **49**, 2204–2206 (2013).
27. Manthiram, A., Yu, X. & Wang, S. Lithium battery chemistries enabled by solid-state electrolytes. *Nat. Rev. Mater.* **2**, 16103 (2017).
28. Zhao, Q., Stalin, S., Zhao, C. Z. & Archer, L. A. Designing solid-state electrolytes for safe, energy-dense batteries. *Nat. Rev. Mater.* **5**, 229–252 (2020).
29. Liu, C., Chi, X., Han, Q. & Liu, Y. A high energy density aqueous battery achieved by dual dissolution/deposition reactions separated in acid-alkaline electrolyte. *Adv. Energy Mater.* **10**, 1903589 (2020).
30. Yu, F. et al. Aqueous alkaline–acid hybrid electrolyte for zinc-bromine battery with 3V voltage window. *Energy Storage Mater.* **19**, 56–61 (2019).
This paper reports a decoupled Zn–Br battery based on a bipolar membrane.
31. Ding, Y., Cai, P. & Wen, Z. Electrochemical neutralization energy: from concept to devices. *Chem. Soc. Rev.* **50**, 1495–1511 (2021).
32. Epsztein, R., Shaulsky, E., Qin, M. & Elimelech, M. Activation behavior for ion permeation in ion-exchange membranes: role of ion dehydration in selective transport. *J. Membr. Sci.* **580**, 316–326 (2019).
33. Feng, J. D. et al. Single-layer MoS_2 nanopores as nanopower generators. *Nature* **536**, 197–200 (2016).
34. Kordesh, K. & Weissenbacher, M. Rechargeable alkaline manganese dioxide/zinc batteries. *J. Power Sources* **51**, 61–78 (1994).
35. Ovshinsky, S. R., Fetcenko, M. A. & Ross, J. A nickel metal hydride battery for electric vehicles. *Science* **260**, 176–181 (1993).
36. Putois, F. Market for nickel-cadmium batteries. *J. Power Sources* **57**, 67–70 (1995).

37. Ji, H. et al. Capacitance of carbon-based electrical double-layer capacitors. *Nat. Commun.* **5**, 3317 (2014).
38. Fleischmann, S. et al. Pseudocapacitance: from fundamental understanding to high power energy storage materials. *Chem. Rev.* **120**, 6738–6782 (2020).
39. Wang, X., Xie, Y., Tang, K., Wang, C. & Yan, C. Redox chemistry of molybdenum trioxide for ultrafast hydrogen-ion storage. *Angew. Chem. Int. Ed.* **57**, 11569–11573 (2018).
40. Hong, J. J. et al. A dual plating battery with the iodine/$[\mathrm{ZnI}_x(\mathrm{OH}_2)_{4-x}]^{2-x}$ cathode. *Angew. Chem. Int. Ed.* **58**, 15910–15915 (2019).
41. Choi, C. et al. Achieving high energy density and high power density with pseudocapacitive materials. *Nat. Rev. Mater.* **5**, 5–19 (2020).
42. Qian, J. et al. High rate and stable cycling of lithium metal anode. *Nat. Commun.* **6**, 6362 (2015).
43. Sun, Y., Liu, N. & Cui, Y. Promises and challenges of nanomaterials for lithium-based rechargeable batteries. *Nat. Energy* **1**, 16071 (2016).
44. Wang, Y. et al. Biomass derived carbon as binder-free electrode materials for supercapacitors. *Carbon* **155**, 706–726 (2019).
45. Cai, Z. et al. Chemically resistant Cu–Zn/Zn composite anode for long cycling aqueous batteries. *Energy Storage Mater.* **27**, 205–211 (2020).
46. Lee, J. H. et al. High-energy efficiency membraneless flowless Zn–Br battery: utilizing the electrochemical–chemical growth of polybromides. *Adv. Mater.* **31**, 1904524 (2019).
47. Liu, T., Wei, X., Nie, Z., Sprenkle, V. & Wang, W. A total organic aqueous redox flow battery employing a low cost and sustainable methyl viologen anolyte and 4-HO-TEMPO catholyte. *Adv. Energy Mater.* **6**, 1501449 (2016).
48. Lin, K. et al. Alkaline quinone flow battery. *Science* **349**, 1529–1532 (2015).
49. Tian, H. et al. High power rechargeable magnesium/iodine battery chemistry. *Nat. Commun.* **8**, 14083 (2017).
50. Gurieff, N., Timchenko, V. & Menictas, C. Variable porous electrode compression for redox flow battery systems. *Batteries* **4**, 53 (2018).
51. Peng, Z., Freunberger, S. A., Chen, Y. & Bruce, P. G. A reversible and higher-rate Li-O_2 battery. *Science* **337**, 563–566 (2012).
52. Qiao, Y. et al. Li-CO_2 electrochemistry: a new strategy for CO_2 fixation and energy storage. *Joule* **1**, 359–370 (2017).
53. Ma, J. L., Bao, D., Shi, M. M., Yan, J. M. & Zhang, X. B. Reversible nitrogen fixation based on a rechargeable lithium-nitrogen battery for energy storage. *Chem* **2**, 525–532 (2017).
54. Huang, Z. F. et al. Design of efficient bifunctional oxygen reduction/evolution electrocatalyst: recent advances and perspectives. *Adv. Energy Mater.* **7**, 1700544 (2017).
55. Xu, W., Lu, Z., Sun, X., Jiang, L. & Duan, X. Superwetting electrodes for gas-involving electrocatalysis. *Acc. Chem. Res.* **51**, 1590–1598 (2018).
56. Maja, M., Orecchia, C., Strano, M., Tosco, P. & Vanni, M. Effect of structure of the electrical performance of gas diffusion electrodes for metal air batteries. *Electrochim. Acta* **46**, 423–432 (2000).
57. Lee, W. K., Ho, C. H., Van Zee, J. W. & Murthy, M. The effects of compression and gas diffusion layers on the performance of a PEM fuel cell. *J. Power Sources* **84**, 45–51 (1999).
58. Pan, J. et al. Advanced architectures and relatives of air electrodes in Zn–air batteries. *Adv. Sci.* **5**, 1700691 (2018).
59. Sun, W. et al. A rechargeable zinc-air battery based on zinc peroxide chemistry. *Science* **371**, 46–51 (2021).
60. Goodenough, J. B. & Park, K. S. The Li-ion rechargeable battery: a perspective. *J. Am. Chem. Soc.* **135**, 1167–1176 (2013).
61. Yuan, L. X. et al. Development and challenges of $LiFePO_4$ cathode material for lithium-ion batteries. *Energy Environ. Sci.* **4**, 269–284 (2011).
62. Chao, D. & Qiao, S. Z. Toward high-voltage aqueous batteries: super- or low-concentrated electrolyte? *Joule* **4**, 1846–1851 (2020).
63. Shen, Y. & Kordesch, K. The mechanism of capacity fade of rechargeable alkaline manganese dioxide zinc cells. *J. Power Sources* **87**, 162–166 (2000).
64. Winter, M. & Brodd, R. J. What are batteries, fuel cells, and supercapacitors? *Chem. Rev.* **104**, 4245–4270 (2004).
65. Donne, S. W., Lawrance, G. A. & Swinkels, D. A. Redox processes at the manganese dioxide electrode: I. constant-current intermittent discharge. *J. Electrochem. Soc.* **144**, 2949–2953 (1997).
66. Gibson, A. J. et al. Dynamic electrodeposition of manganese dioxide: temporal variation in the electrodeposition mechanism. *J. Electrochem. Soc.* **163**, H305 (2016).
67. Singh, A. et al. Towards a high MnO_2 loading and gravimetric capacity from proton-coupled Mn^{4+}/Mn^{2+} reactions using a 3D free-standing conducting scaffold. *J. Mater. Chem. A* **9**, 1500–1506 (2021).
68. Xu, Y. et al. High-voltage rechargeable alkali–acid Zn–PbO_2 hybrid battery. *Angew. Chem. Int. Ed.* **59**, 23593–23597 (2020).
69. Noack, J., Roznyatovskaya, N., Herr, T. & Fischer, P. The chemistry of redox-flow batteries. *Angew. Chem. Int. Ed.* **54**, 9776–9809 (2015).
70. Khor, A. et al. Review of zinc-based hybrid flow batteries: from fundamentals to applications. *Mater. Today Energy* **8**, 80–108 (2018).
71. Chang, Z. et al. Rechargeable Li//Br battery: a promising platform for post lithium ion batteries. *J. Mater. Chem. A* **2**, 19444–19450 (2014).
72. Bai, P., Viswanathan, V. & Bazant, M. Z. A dual-mode rechargeable lithium–bromine/oxygen fuel cell. *J. Mater. Chem. A* **3**, 14165–14172 (2015).
73. Bray, W. C. The hydrolysis of iodine and bromine. *J. Am. Chem. Soc.* **32**, 932–938 (1910).
74. Jones, G. & Baeckström, S. The standard potential of the bromine electrode. *J. Am. Chem. Soc.* **56**, 1524–1528 (1934).
75. Fischer, J. & Bingle, J. The vapor pressure of bromine from 24 to 116 °. *J. Am. Chem. Soc.* **77**, 6511–6512 (1955).
76. Küttinger, M., Loichet Torres, P. A., Meyer, E., Fischer, P. & Tübke, J. Systematic study of quaternary ammonium cations for bromine sequestering application in high energy density electrolytes for hydrogen bromine redox flow batteries. *Molecules* **26**, 2721 (2021).
77. Hoobin, P. M., Cathro, K. J. & Niere, J. O. Stability of zinc/bromine battery electrolytes. *J. Appl. Electrochem.* **19**, 943–945 (1989).
78. Kautek, W. In situ investigations of bromine-storing complex formation in a zinc-flow battery at gold electrodes. *J. Electrochem. Soc.* **146**, 3211–3216 (1999).
79. Eustace, D. J. Bromine complexation in zinc-bromine circulating batteries. *J. Electrochem. Soc.* **127**, 528–532 (1980).
80. Li, Y. et al. Advanced zinc-air batteries based on high-performance hybrid electrocatalysts. *Nat. Commun.* **4**, 1805 (2013).
81. Li, Y. & Dai, H. Recent advances in zinc–air batteries. *Chem. Soc. Rev.* **43**, 5257–5275 (2014).
82. Fu, J. et al. Electrically rechargeable zinc–air batteries: progress, challenges, and perspectives. *Adv. Mater.* **29**, 1604685 (2017).
83. Lee, D. U., Choi, J. Y., Feng, K., Park, H. W. & Chen, Z. Advanced extremely durable 3D bifunctional air electrodes for rechargeable zinc-air batteries. *Adv. Energy Mater.* **4**, 1301389 (2014).
84. Zhang, J., Zhao, Z., Xia, Z. & Dai, L. A metal-free bifunctional electrocatalyst for oxygen reduction and oxygen evolution reactions. *Nat. Nanotechnol.* **10**, 444–452 (2015).
85. Geng, D. et al. From lithium-oxygen to lithium-air batteries: challenges and opportunities. *Adv. Energy Mater.* **6**, 1502164 (2016).
86. Lin, C. et al. High-voltage asymmetric metal–air batteries based on polymeric single-Zn^{2+}-ion conductor. *Matter* **4**, 1287–1304 (2021).
This paper designs a polymeric single-Zn^{2+}-ion conductor, making high-voltage decoupled metal–air batteries possible.
87. Zhang, L. & Lin, Z. Higher-voltage asymmetric-electrolyte metal-air batteries. *Joule* **5**, 1325–1327 (2021).
88. Matter, P. H. & Ozkan, U. S. Non-metal catalysts for dioxygen reduction in an acidic electrolyte. *Catal. Lett.* **109**, 115–123 (2006).
89. Li, L. & Manthiram, A. Decoupled bifunctional air electrodes for high-performance hybrid lithium-air batteries. *Nano Energy* **9**, 94–100 (2014).
90. Yu, X. & Manthiram, A. A voltage-enhanced, low-cost aqueous iron–air battery enabled with a mediator-ion solid electrolyte. *ACS Energy Lett.* **2**, 1050–1055 (2017).
91. Wen, H. et al. Ultrahigh voltage and energy density aluminum-air battery based on aqueous alkaline-acid hybrid electrolyte. *Int. J. Energy Res.* **44**, 10652–10661 (2020).
92. Xu, K. Diffusionless charge transfer. *Nat. Energy* **4**, 93–94 (2019).
93. Xie, F. et al. Mechanism for zincophilic sites on zinc-metal anode hosts in aqueous batteries. *Adv. Energy Mater.* **11**, 2003419 (2021).
94. Yuan, L. et al. Regulation methods for the Zn/electrolyte interphase and the effectiveness evaluation in aqueous Zn-ion batteries. *Energy Environ. Sci.* **14**, 5669–5689 (2021).
95. Zhao, S. et al. All-in-one and bipolar-membrane-free acid-alkaline hydrogel electrolytes for flexible high-voltage Zn-air batteries. *Chem. Eng. J.* **430**, 132718 (2022).
96. Gong, K. et al. A zinc–iron redox-flow battery under $100 per kW h of system capital cost. *Energy Environ. Sci.* **8**, 2941–2945 (2015).
97. Li, H., Weng, G., Li, C. Y. V. & Chan, K. Y. Three electrolyte high voltage acid–alkaline hybrid rechargeable battery. *Electrochim. Acta* **56**, 9420–9425 (2011).

Acknowledgements

This work was financially supported by the National Natural Science Foundation of China (grant nos. 21725103, 51522101, 51471075, 51631004 and 51401084), National Key R&D Program of China (grant no. 2019YFA0705700) and the China Postdoctoral Science Foundation (grant no. 2020M681035).

Author contributions

X.Z. and Y.Z. contributed to the writing and editing of all sections of the manuscript. All authors contributed to the research and discussion of data, figure preparation and proofreading of the manuscript.

Competing interests

The authors declare no competing interests.

Peer review information

Nature Reviews Chemistry thanks W. Hu, S. Qiao and the other, anonymous, reviewer(s) for their contribution to the peer review of this work.

Publisher's note